Experimental Assessment of Cryogenic Cooling Impact on Induction Motors

This article has been accepted for publication in IEEE Transactions on Energy Conversion. This is the author's version which has not been fully edited and content may change prior to final publication. Citation information: DOI 10.1109/TEC.2022.3183939

Experimental Assessment of Cryogenic Cooling Impact on Induction Motors

Luís F. D. Bucho, João F. P. Fernandes, *Member, IEEE*, Marco Biasion, *Student Member, IEEE*, Silvio Vaschetto, *Senior Member, IEEE*, Andrea Cavagnino, *Fellow, IEEE*

***Abstract*—In this work, an experimental assessment of the influence of cryogenic cooling in a conventional induction motor is presented. The performance of a fractional kilowatt induction motor is evaluated when submerged in liquid nitrogen. Using the single-phase equivalent electric circuit, the influence of the temperature and skin-effect is analyzed in the variation of the machine's parameters, under ambient and cryogenic conditions. Also, the variation of the iron core and mechanical losses are evaluated. An analytical methodology is proposed to estimate the change of motor performance under cryogenic conditions. For the analyzed induction motor, measurements are performed to verify the predicted machine performance. The experimental tests in cryogenic conditions show the possibility of achieving higher efficiency levels with more than double the nominal torque. Also, due to the cryogenic environment, there was no thermal constraint in the operation of the induction motor.**

***Index Terms*—Cryogenics, electric machines, induction motor, electromagnetic measurements, modeling, testing, loss measurement, performance, skin effect, temperature impact.**

I. Introduction

In the past few years considerable efforts, from the industrial and research communities, have been made towards the electrification of transportation systems. These efforts have been aided by regulatory bodies, which, not only have been imposing higher efficiency standards for the manufacturing and design of new machines, but also identified the need for more measures regarding policy and long-term commitment [1], [2]. The EU, in Flightpath 2050: Europe's Vision for Aviation report, identified the electrification of commercial aircraft as a way to reduce the emissions of CO_2, NO_x and noise, by 75%, 90% and 65%, respectively, by 2050 [3]. This led to the need of higher requirements for electrical machines, such as higher specific torque/power and higher efficiencies. For instance, in the STARC-ABL project from NASA, a target of 13-20 kW/kg is defined for the development of passenger-class aircraft [4].

Current solutions to potentially achieve these challenging power and efficiency targets require the use of new machine topologies or new advanced materials, such as superconductors [5]-[13]. Regarding superconductors, recent studies have shown the possibility of achieving electrical machine designs with 20-30 kW/kg, but still in a limited technology readiness level (TRL) [14], [15].

However, cryogenic cooled machines can be an alternative solution between conventional machines and superconducting ones. The operation of the machines in a cryogenic environment has shown considerable improvements to specific torque and efficiency, due to the decrease of Joule losses and higher loading capacity. Indeed, the decrease in temperature causes a significant reduction in resistivity. Consequently, the resistivity of stator and rotor conductors as well as the iron core lamination resistivity are significantly reduced at cryogenic temperatures [16]. This results in a significant decrease of Joule losses in the stator and rotor conductors, but also an increase in iron core losses, due to eddy current. On the other hand, compared with the eddy current losses increase, the change of the *BH* curve and hysteresis losses of iron cores are significantly lower for cryogenic temperatures [17]-[18]. Despite literature showing that cryogenic conditions allow a higher loading capacity for electric machines, there is still the need for analyzing the balance between the stator, rotor and iron losses, and also the consequences on the mechanical losses.

Cryogenic induction machines (IMs) have been at the forefront of this research due to their high operating reliability in cryogenic environments and their low cost [16]-[20]. In particular, cryogenic IMs are considered a potential design solution to achieve higher specific torque and efficiency values when cryogenic fluids are available or easily implemented. For instance, they have been used in missile cryogenic propellant systems using liquid hydrogen [21], or in the pumping stations of liquified natural gas (approximately 110K) [22]-[24]. When designed to operate under a liquid natural gas environment, the same torque of an air-cooled induction machine can be obtained with about 40% less volume [7].

Following this research topic, in this paper, the performance of a conventional totally enclosed non-ventilated (TENV) 90W IM, designed for ambient temperature operation, is tested under a cryogenic environment. It is important to highlight that, different from cryogenic studies where the machine was designed for cryogenic conditions, here a conventional machine is subject to cryogenic operation, within LN_2 submersion to verify its increase of performance. A small-size machine has been selected to facilitate its wet cryogenic testing, using a vessel containing liquid nitrogen, and to analyze the impact of cryogenic conditions on its equivalent circuit parameters.

Manuscript received XXX XX, 2022; revised XXX XX, 2022 and XXXX XX,2022; accepted XXXX XX, 2022. Date of publication XXX XX, 2022; date of current version XXX XX, 2022. This work was partially financed by national funds through FCT – Foundation for Science and Technology, I.P., through IDMEC, under LAETA, project UIDB/50022/2020. *(Corresponding author: João F. P. Fernandes).*

L. F. D. Bucho and J.F.P. Fernandes are with Departamento de Engenharia Electrotécnica e de Computadores, University of Lisbon, Instituto Superior Técnico, Lisbon, Portugal (e-mail: luis.bucho@tecnico.ulisboa.pt, joao.f.p.fernandes@tecnico.ulisboa.pt). M. Biasion, S. Vaschetto, and A. Cavagnino are with the Politecnico di Torino, Dipartimento di Energia, Turin, 10129, Italy (e-mail: marco.biasion@polito.it, silvio.vaschetto@polito.it, andrea.cavagnino@polito.it).

Color versions of one or more of the figures in this article are available online at https://ieeexplore.ieee.org.Digital Object Identifier XXXXXX.

This article has been accepted for publication in IEEE Transactions on Energy Conversion. This is the author's version which has not been fully edited and content may change prior to final publication. Citation information: DOI 10.1109/TEC.2022.3183939

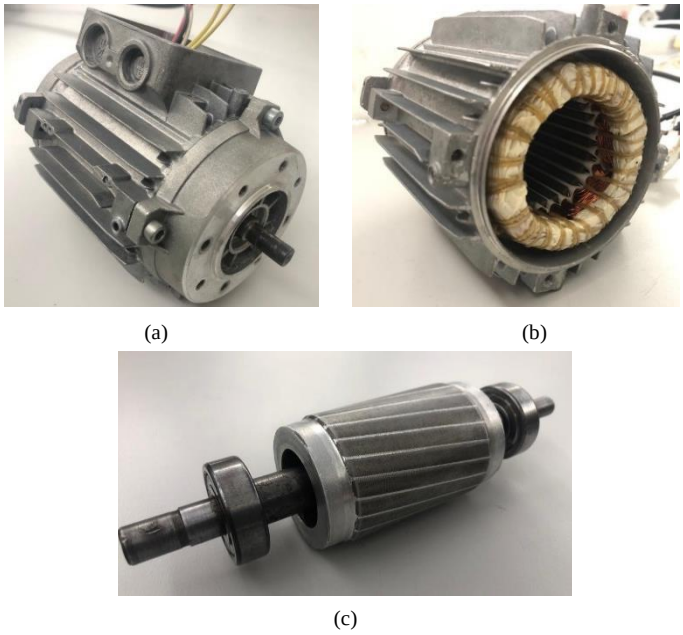

(a) (b)

(c)

Fig. 1. TENV induction machine used for the study. (a) overview, (b) the stator and (c) the rotor.

TABLE I
NOMINAL VALUES AND DESCRIPTION OF THE TESTED MACHINE

Induction machine	Rated Values
Voltage, (V)	40
Current, (A)	3.6
Power, (W)	90
Speed, (rpm)	1350
Frequency, (Hz)	50
cos(φ)	0.61
Materials	
Rotor cage	Aluminum die-cast
Stator windings	Copper distributed
Iron core	FeSi Alloy

An experimental setup was developed to test this machine under cryogenic conditions with different loads. An analytical model based on the Steinmetz equivalent circuit is also applied to verify the influence of the cryogenic temperature and skin-effect on the machine performance. Furthermore, the influence of cryogenic conditions on the machine equivalent parameters is also estimated and discussed.

II. MODELING THE IMPACT OF TEMPERATURE ON MACHINE PARAMETERS AND PERFORMANCE

The impact of cryogenic cooling on the performance of induction machines is first analyzed based on the equivalent circuit parameters variation. This analysis is done for a conventional 90 W, 40 V, 50 Hz, four-pole machine, which is submerged in liquid nitrogen (77K) Figure 1 and Table I show the machine and its main characteristics, respectively. From now on, the induction machine at ambient temperature is referred to as the reference one (REF), and the cryogenic one as (CRYO) when submerged in liquid nitrogen (77K).

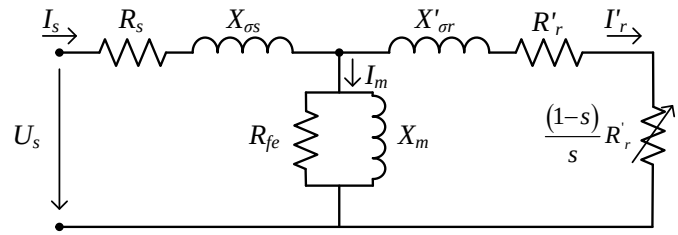

Fig. 2. Single-phase equivalent circuit.

To support the experimental findings, analytical calculations are done based on the methodology presented in [25] to consider the variation of the IM single-phase equivalent circuit's parameters shown in Fig. 2. Based on the parameters obtained by the experimental tests at ambient temperature, the influence of the cryogenic temperature and skin effect is analyzed, and the new parameters at cryogenic conditions are estimated and verified by experiments at 77K.

A. Stator resistance R_s and reactance $X_{\sigma s}$

The stator of the machine under analysis is equipped with a conventional three-phase distributed winding made of copper wires with a 1 mm diameter. Changing the temperature from the nominal one, at ambient temperature conditions, to a cryogenic environment, impacts the electric resistivity of the copper. The copper presents a linear resistivity with the temperature from around 55K [26]. Therefore, the calculation of the *dc* value of the stator resistance at cryogenic conditions can be done using the linear variation of the copper electric resistivity in (1).

$$\rho(T)=\rho_0\left(1+\alpha_{cu}\left(T-T_0\right)\right) \tag{1}$$

In (1), ρ is the material's resistivity at a given temperature T, ρ_0 is the resistivity at the reference temperature T_0, and α_{cu} is the material temperature coefficient.

From experimental tests at rated supply and load conditions, measurements of the stator winding temperature indicate a working temperature of 41ºC (314K) and 77K, for ambient and cryogenic conditions, respectively. Considering α_{cu} = 0.00386 and a reference copper resistivity of $\rho_0 = 1.68\cdot10^{-8}\,\Omega$m at T_0 = 20°C, the resistivity values for the ambient and cryogenic conditions are $\rho_{amb} = 1.816\cdot10^{-8}\,\Omega$m and $\rho_{cryo} = 0.279\cdot10^{-8}\,\Omega$m, respectively. This corresponds to a decrease of 84.6% of the electric resistivity in cryogenic conditions. Regarding the stator reactance, there is no expected direct influence of the temperature in the distribution of the magnetic leakage flux, and therefore, in its reactance [23], [27].

For the calculation of the skin effect, the temperature effect on the change of the material electric conductivity must be considered. For the winding temperature of 41ºC (REF) and 77K (CRYO), and an electric frequency of 50 Hz, the values of the skin depth are 9.6 mm and 3.8 mm, respectively. As these values are larger than the copper wire diameter used, the skin effect can be neglected, both for the stator resistivity and reactance.

This article has been accepted for publication in IEEE Transactions on Energy Conversion. This is the author's version which has not been fully edited and content may change prior to final publication. Citation information: DOI 10.1109/TEC.2022.3183939

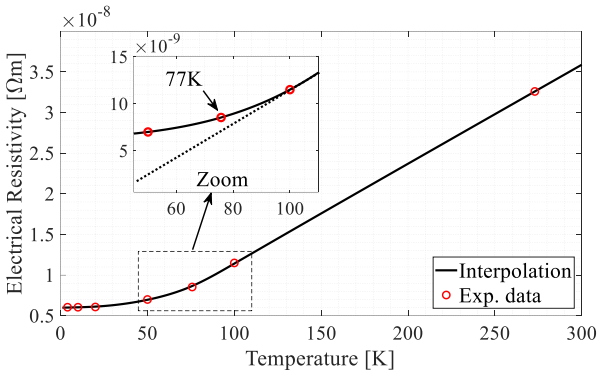

Fig. 3. Electric resistivity of the aluminum alloy 2024-0 with the temperature.

B. Rotor resistance R'_r and reactance $X'_{\sigma r}$

The equivalent rotor resistance R'_r can be expressed by (2), where K_R is the skin-effect coefficient for the rotor bar resistance, $R_{b,DC}$ is the *dc* resistance of the rotor bar, R_a is the *dc* resistance of the end-ring, N_{bars} is the number of rotor cage bars and β_r is the angle between two adjacent rotor bars [28]. The parameter K_{RS} reports the rotor resistance to the stator side, where Z_{ph} and $k_{w,1}$ are the number of conductors in series per phase and the fundamental winding factor of the stator winding, respectively. While the change of temperature is considered on both rotor bars and end-rings *dc* resistances, the skin-effect is only associated with the rotor's bars. Typically, the skin effect on the end-rings is considered negligible [28].

$$R'_r(\theta) = K_{RS} \cdot \left(K_R(\theta) \cdot R_{b,DC}(\theta) + \frac{2R_a(\theta)}{4N_{bars}\mathrm{sen}^2\left(\frac{\beta_r}{2}\right)} \right), \quad (2)$$

$$K_{RS} = \frac{3}{N_{bars}} \left(Z_{ph} \cdot k_{w,1} \right)^2$$

The determination of the *dc* resistance of the rotor bars and end-rings only depends on their geometry and the material resistivity. In this case, the rotor cage is made of the aluminum die-cast alloy 2024-0. Figure 3 shows the evolution of the material's electric resistivity with the temperature between 0K and 300K (27°C) [29]. As evident, this material does not present a linear variation of electrical resistivity for the whole range of temperatures experienced in this work.

The skin-effect coefficient, K_R, must be computed considering the shape of the rotor bar cross-section and the rotor electric frequency. The procedure presented in [28] can be used, by dividing the rotor bar cross-section into multiple rectangular layers and applying the Ampère and Faraday laws. Considering the resistance and inductance of each layer, the current distribution can be computed, starting from the bottom layer, and the final *ac* power losses and magnetic energy distribution are compared with the *dc* ones. The skin-effect coefficients for the rotor resistance, K_R, and the leakage reactance, K_L, can be obtained using (3) and (4), where n is the number of layers, R_i and L_i are the resistance and inductance of each layer and $I_{i,ac}$ and $I_{i,dc}$ are the *ac* and *dc* currents at each layer, i.

$$K_R(\theta) = \frac{P_{ac}}{P_{dc}} = \frac{\sum_{i=1}^{n} R_i \left| I_{i,ac} \right|^2}{\sum_{i=1}^{n} R_i I_{i,dc}^{\ 2}} \quad (3)$$

$$K_L(\theta) = \frac{W_{m,ac}}{W_{m,dc}} = \frac{\sum_{i=1}^{n} L_i \left| \sum_{k=1}^{p} I_{k,ac} \right|^2}{\sum_{i=1}^{n} L_i \left| \sum_{k=1}^{p} I_{k,dc} \right|^2} \quad (4)$$

Similarly, the impact of skin-effect on the rotor leakage reactance is only considered for the rotor slot part. Therefore, the rotor leakage reactance must be divided into its components as in (5), where X_{leak_airgap} represents the slotting effect and the distribution of the stator winding along the circumference of the air gap, X_{end_ring} is the leakage reactance of the end-ring, X_{slot} is the rotor slot leakage reactance and $X_{leak,skew}$ represents the influence of the skewing of the rotor bars [30].

$$X'_{\sigma r} = K_{RS} \left(X_{leak\_airgap} + X_{end\_ring} + X_{slot}(\theta) + X_{leak,skew} \right) \quad (5)$$

Hence, the leakage reactance component related to the rotor slots can be corrected with the skin-effect coefficient, $X_{slot}(\theta) = K_L(\theta) \cdot X_{slot\_dc}$.

C. Equivalent iron losses resistance R_{fe} and magnetizing reactance X_m

The iron core in electrical machines can be made of a wide range of electric steels. These different electric steels vary from impurities content to grain size and orientation, and even by the cutting and annealing process used in manufacturing. Therefore, for each electric steel, the increase of iron losses must be analyzed.

It is known that the effect of temperature in the iron core is due, for the most part, to the increase of electric conductivity, associated with the eddy current losses and, to a smaller extent, associated with the hysteresis losses [31]. As identified in [25] and [31], for typical laminated iron core materials, such as M400-50A and M43, there is an increase between 10 % to 16 % of iron losses when the magnetic core is submerged in liquid nitrogen, at a frequency of 50 Hz. Therefore, as a first approximation, in this research activity the hysteresis losses contributions were considered constant with the temperature.

Regarding the magnetizing reactance, since it mostly represents the magnetic energy in the air gap, the influence of the temperature is considered to be negligible [23].

III. Experimental Setup

Experimental tests were carried out to evaluate the influence of the cryogenic environment in the 90W induction machine originally designed for being operated at ambient temperature, and to validate the proposed methodology for assessing the impact of such low temperatures on the machine performance.

To this purpose, both ambient temperature and cryogenic experimental tests were performed using the experimental setup shown in Fig. 4.

This article has been accepted for publication in IEEE Transactions on Energy Conversion. This is the author's version which has not been fully edited and content may change prior to final publication. Citation information: DOI 10.1109/TEC.2022.3183939

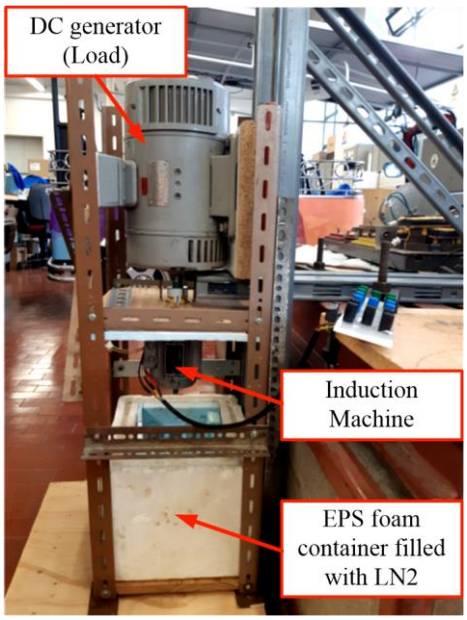

Fig. 4. Experimental setup to test the induction machine.

Fig. 5. Grease removal process from the bearings.

Under cryogenic tests, the IM under analysis was kept immersed in liquid nitrogen in an expanded polystyrene (EPS) foam container. The setup was developed in a vertical position to facilitate the mechanical coupling between the induction machine and the 1kW calibrated DC machine used as load. The speed was acquired using a tachometer coupled to the DC machine axis, while the input power of the induction machine was measured using a data acquisition system that records each phase voltage and current.

Before starting the cryogenic tests, the motor bearings required treatment. In fact, most lubricants used today in standard bearings can handle a very wide spectrum of temperatures, usually from -50ºC up to 200ºC, but its grease freezes under LN_2 temperature. Therefore, the grease had to be removed using an acetone bath. In detail, the bearings are left inside the acetone bath for about 5 days, to completely remove any residue of grease. Every day the acetone was changed, and the bearings tested, by immersion in liquid nitrogen, until it is possible to rotate them freely with no apparent formation of ice crystals – see Fig. 5.

Moreover, the IM had some holes drilled in the cover to allow the liquid nitrogen to be in contact with its active parts and to effectively keep them at cryogenic temperatures, Fig. 6. Please note that the LN2 has good lubricant properties, and that the vertical mounting helps to reduce the bearings heating during the ambient temperature tests in air.

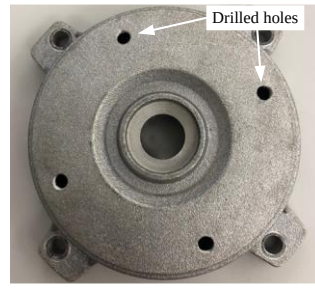

Fig. 6. Drilled holes in the IM cover to allow liquid nitrogen inside.

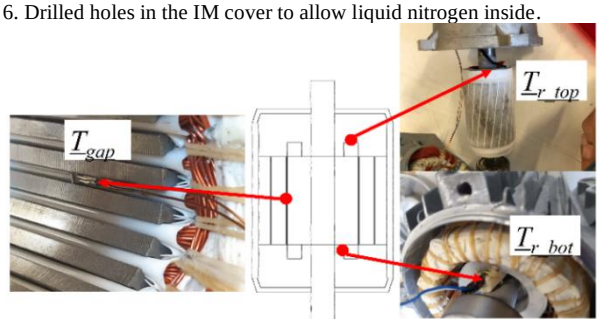

Fig. 7. Position of cryogenic temperature sensors.

IV. Experimental Tests and Results

To experimentally characterize the IM, no-load, locked rotor and load tests were conducted both at ambient and cryogenic temperatures. To verify the temperature of the machine's active parts under cryogenic conditions, the stator and rotor temperatures during the testing activity were measured using cryogenic temperature sensors.

The locked rotor test was performed for approximately 1 hour, with different values of stator current, up to 3.6A at ambient temperature and up to 10 A at cryogenic conditions. As Fig. 7 shows, during this test three cryogenic temperature sensors were used to monitor the temperatures at the machine air gap (T_{gap}), at the top and at the bottom surfaces of the rotor (T_{r_top} and T_{r_bot}), respectively. While for the locked rotor test T_{r_top} and T_{r_bot} sensors were in contact with the rotor surface, for the no-load test only the T_{r_top} sensor, positioned at 1 mm over the rotor surface, was used. In particular, the temperature sensor at the air gap had also to be removed because of the small air gap length of the tested IM (about 0.3 mm), that was approximately the same thickness as the cryogenic sensor.

Results from the conducted tests show that the temperature of the machine, immersed in liquid nitrogen, is lower than the boiling temperature of the liquid nitrogen, i.e., 77K. In Fig. 8 is shown the evolution of the temperature during the locked rotor tests. There is a small gradient of temperature between the bottom and top surfaces of the rotor (less than 1K), but temperatures are lower than 77K. Since during the no-load test the air gap temperature was not measured, it was not possible to verify if vapor nitrogen was present in the air gap. However, the maximum temperature measured by the top sensor was lower than 77K.

Therefore, the experimental results indicate that under cryogenic conditions the active parts of the IM remain close to 77K. Thus, this temperature value can be used for applying the proposed methodology for the estimation of the induction machine equivalent parameters at cryogenic conditions.

This article has been accepted for publication in IEEE Transactions on Energy Conversion. This is the author's version which has not been fully edited and content may change prior to final publication. Citation information: DOI 10.1109/TEC.2022.3183939

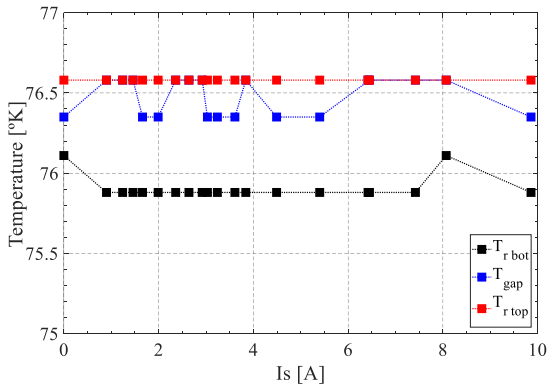

Fig. 8. No-load test. Temperature of cryogenic sensors at the airgap (T_{gap}) and at the top (T_{r_top}) and bottom (T_{r_bot}) of the rotor.

A. Equivalent circuit parameters determination

From the no-load and locked rotor tests, the equivalent circuit parameters of the IM were estimated according to the IEC 60034-2-1 procedure, both for ambient and cryogenic conditions. In particular, no-load tests were performed by applying different values of stator voltage, starting slightly above the rated voltage and decreasing its value until about 20 % of its rated value. The same procedure was applied for the locked rotor tests, but with lower stator currents obtained by applying reduced voltage levels.

Figure 9 and Fig. 10 report the measured mechanical and iron losses and reactive power, respectively, both for ambient and cryogenic conditions, while Table II lists the obtained equivalent circuit parameters and the mechanical losses. The results for the no-load tests show an increase of mechanical losses from 1.96 W, at ambient temperature, to 3.83 W, at cryogenic conditions, both without the bearing grease, Fig. 9(a). Moreover, for the same level of magnetization, the iron losses increased about 11.6 % under cryogenic conditions, corresponding to a decrease of 10.4 % of the equivalent iron losses resistance. For the magnetizing reactance, deviations between the ambient temperature and cryogenic results are negligible (deviation of 1.2 %), as also evident by the measured reactive power in Fig. 9(b).

From the locked rotor tests, the stator and rotor resistances and reactances were estimated. In particular, the stator resistance was measured before and after the experimental tests, and an equal division between the stator and rotor reactances was considered, $X_S = X'_R$.

The values measured for the stator resistance are equal to 1.1 Ω and 0.175 Ω for the ambient and the cryogenic temperature, respectively. This corresponds to a decrease of 84.1 %, when operating under cryogenic conditions, validating the proposed model for the stator resistance calculation proposed in Section II.A, where a decrease of 84.6 % was expected. Regarding the stator and rotor reactances, a negligible difference is found between the ambient temperature and cryogenic conditions, again as expected. For the rotor resistance, a reduction of 73.4% has been obtained from ambient temperature to cryogenic conditions.

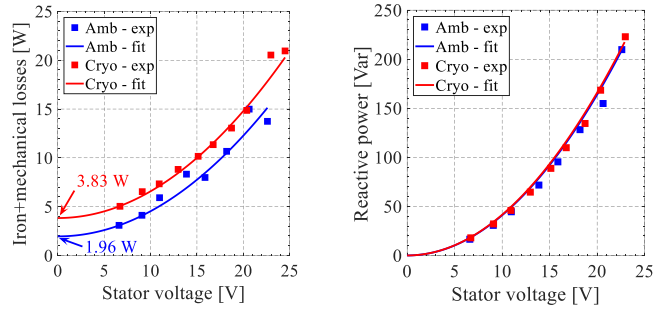

(a) (b)

Fig. 9. No-load results: (a) mechanical and iron losses and (b) reactive power as a function.

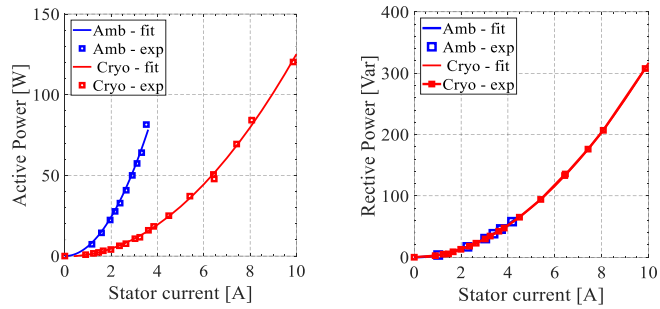

(a) (b)

Fig. 10 Locked rotor results: (a) active power and (b) reactive power, as a function of the stator current.

TABLE II
EQUIVALENT CIRCUIT PARAMETERS AND MECHANICAL LOSSES FOR THE TESTED IM AT AMBIENT AND CRYOGENIC TEMPERATURES

Parameter	Amb. Temp. (20°C)	Cryo. Temp. (77K)	Difference
R_{fe}, (Ω)	116.4	104.3	-10.4%
X_m, (Ω)	7.33	7.24	-1.2%
R_S, (Ω)	1.10	0.175	-84.1%
R'_R, (Ω)	0.914	0.240	-73.4%
X_S, (Ω)	0.532	0.532	+0.0%
X'_R, (Ω)	0.532	0.532	+0.0%
P_{losses_mec}, (W)	1.96	3.83	+95.4%

Using the proposed methodology, the analytical estimation of the rotor resistance is presented, starting with its measured value at ambient temperature, and verified with experimental measurements at cryogenic conditions. At ambient conditions, using the analytical model in (1) to (5), the predicted rotor temperature was 61ºC, resulting in around 20°C difference with respect to the stator winding as typical for TENV induction motors. At this working temperature, the aluminum electric resistivity is $\rho_{al\_amb} = 3.24 \cdot 10^{-8}$ Ωm (obtained from Fig. 3), and the skin effect coefficients for the locked rotor condition are $K_R = 1.003$ and $K_L = 0.9993$.

With these values, the skin effect can be neglected at ambient temperature conditions and the estimated *ac* rotor resistance is

$$R'_{r\_dc}(61^{o}C) = R'_{r\_ac}(61^{o}C) = 0.914\,\Omega \qquad (6)$$

When operating under cryogenic temperature, with a temperature of 77K, the aluminum resistivity will decrease to $\rho_{al\_amb} = 0.789 \cdot 10^{-8}$ Ωm (obtained using Fig. 3), and the *dc* rotor resistance can be estimated using (7). With (2), the *dc* rotor

This article has been accepted for publication in IEEE Transactions on Energy Conversion. This is the author's version which has not been fully edited and content may change prior to final publication. Citation information: DOI 10.1109/TEC.2022.3183939

resistance can be divided into rotor bar and end-rings resistance, as shown in (8). With this, the skin-effect coefficient, K_R, can be applied to the rotor bar slot component.

$$R'_{r\_dc}\left(77^{o}\,\mathrm{K}\right)=\frac{\rho_{al}\left(77^{o}\,\mathrm{K}\right)}{\rho_{al}\left(61^{o}\,\mathrm{C}\right)}R'_{r\_dc}\left(61^{o}\,\mathrm{C}\right)=0.223\Omega \quad (7)$$

$$R'_{r\_dc}\left(77^{o}\,\mathrm{K}\right)=0.223\Omega=\underset{bars}{0.131}+\underset{end-rings}{0.092} \quad (8)$$

At cryogenic conditions with the locked-rotor, the skin-effect coefficient is K_R = 1.055 and the estimated *ac* rotor resistance is

$$R'_{r\_ac}\left(77^{o}\,\mathrm{K}\right)=K_R\,\underset{bars}{0.131}+\underset{end-rings}{0.092}=0.230\Omega \quad (9)$$

As it can be seen, the deviation between the estimated rotor resistance, 0.230Ω, and the experimentally one, 0.240Ω, is about 4.2%, thus verifying the proposed methodology.

B. Mechanical losses

After evaluating the performance of the induction machine under cryogenic conditions, a study of the experimental mechanical losses was performed for different electric frequencies. The induction machine was tested under 20, 30, 40 and 50 Hz. The stator voltage was regulated to assure the same magnetizing flux for all frequencies. Results in Fig. 11 show that there is an increase in mechanical losses under cryogenic conditions, with an average offset of 1.83 W. These drag losses are due to the friction with LN_2.

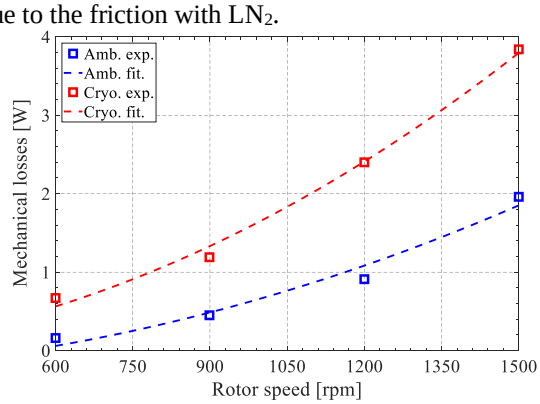

Fig. 11. Comparison between ambient temperature and cryogenic mechanical losses for different frequencies.

C. Load tests

The IM torque-speed curve was experimentally obtained through load tests and compared with the one obtained using the estimated equivalent parameters from the proposed methodology, for both ambient and cryogenic conditions. To verify the stability of the IM when submerged in liquid nitrogen, load tests were performed for 1 hour. During this test, the machine operated without experiencing abnormal vibrations.

Figure 12 shows the torque-speed characteristics, while Fig. 13 presents the efficiency-speed curves. At ambient temperature operation, the maximum current was limited to the rated one. The maximum efficiency of 63% was obtained for a stator current of 3.3 A, a torque of 0.72 Nm and a speed of 1353 rpm, corresponding to a mechanical power equal to 102 W. Under these conditions, the stator and rotor Joule losses, the iron losses and the mechanical losses correspond to 35.9 W, 9.6 W, 12.5 W and 1.96 W, respectively.

Under cryogenic conditions, the stator current was not limited. Therefore, the whole stable zone of the torque-speed curve could be measured. The maximum efficiency of 85.2% was obtained for a stator current of 6.7 A, a torque of 1.95 Nm and a speed of 1441 rpm, and a mechanical power of 294.3 W.

When compared with the ambient temperature operation, there is an increase of 171% of nominal torque and 189% of nominal mechanical power. Due to the high reduction of stator and rotor resistances, the impact of these losses on the machine operation is drastically lower. In Table III and Fig. 14 the performance of the induction machine under ambient temperature and cryogenic conditions, at the maximum efficiency point, is compared. These results were obtained based on experimental tests and the calibrated analytical model (equivalent circuit). The stator current, torque and speed were obtained experimentally, and the segregation of the losses was obtained based on the calibrated analytical model according to the IEC 60034-2-1 Standard procedures for ambient temperature operation. In addition, is also shown a comparison of performances and losses for cryogenic conditions with the same rated torque of the ambient temperature operation, Fig 14 and Fig. 15 and Table III. For the same torque, under cryogenic conditions the efficiency increases from 63.0% to 79.7%, mostly due to stator and rotor losses reduction. There is a slight increase of stator current due to the increase of the no-load current (I_{0amb} = 2.5 A for ambient and I_{0cryo} = 3.0 A for cryogenic conditions) due to the higher iron losses and a higher magnetizing current due to the higher magnetization level of the machine core because of the reduced stator voltage drop.

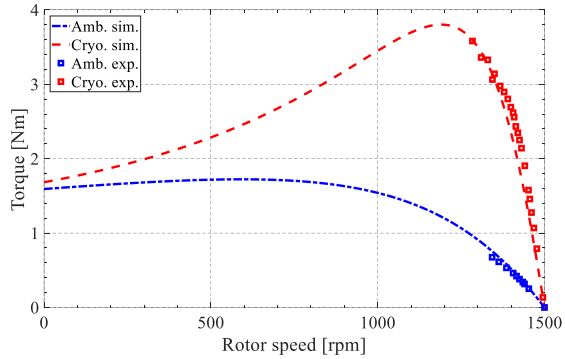

Fig. 12. Toque as a function of the rotor speed for the investigated IM.

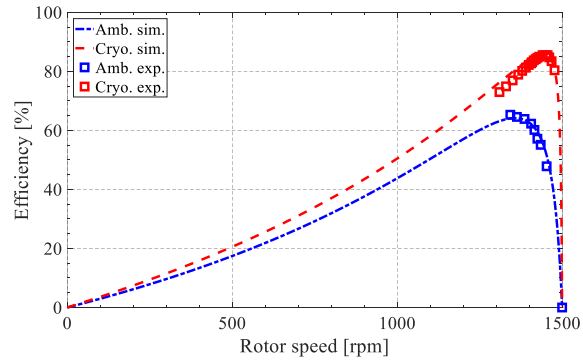

Fig. 13. Efficiency as a function of the rotor speed for the investigated IM.

This article has been accepted for publication in IEEE Transactions on Energy Conversion. This is the author's version which has not been fully edited and content may change prior to final publication. Citation information: DOI 10.1109/TEC.2022.3183939

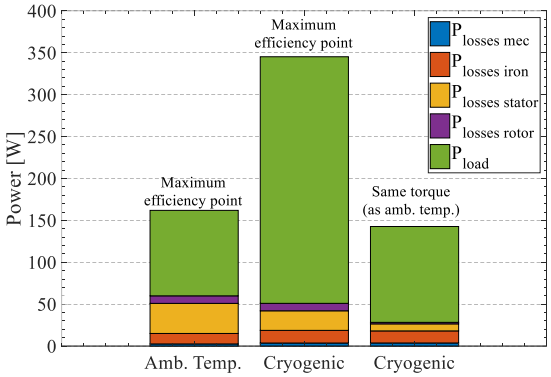

Fig. 14. Comparison between ambient temperature and cryogenic performances at maximum efficiency and same torque.

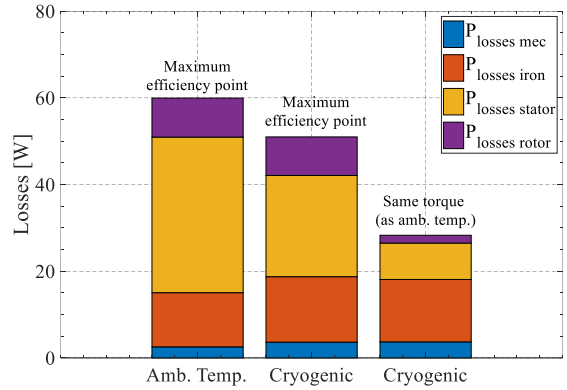

Fig. 15. Comparison of losses between ambient temperature and cryogenic performances at maximum efficiency and same torque.

TABLE III
SUMMARIZED PERFORMANCE FOR THE TESTED IM AT MAXIMUM EFFICIENCY POINT AND AT SAME TORQUE FOR AMBIENT AND CRYOGENIC OPERATIONS (% VARIATIONS WITH RESPECT TO AMBIENT CONDITIONS)

	Ambient temperature.	Cryogenic temperature			
		@ max. efficiency		@ same torque	
Maximum efficiency, (%)	63.0 (s=10.9%)	85.2 (s=4%)	+35%	79.7 (s=1.5%)	+16.7%
Stator current, (A)	3.3	6.7	+103%	4.0	+21%
Torque, (Nm)	0.72	1.95	+171%	0.72	
Rotor speed, (rpm)	1353	1441	+7%	1477	+9%
Mechanical output Power, (W)	102.0	294.3	+189%	111.4	+9%
Mechanical losses, (W)	1.96	3.83	+95%	3.7	+89%
Iron losses, (W)	12.5	14.5	+16%	14.4	+15%
Stator Joule losses, (W)	35.9	23.3	-35%	8.4	-77%
Rotor Joule losses, (W)	9.6	9.5	-1%	1.8	-81%

In addition, under cryogenic conditions, the maximum mechanical power was 481.5 W (3.8 Nm) with an efficiency of 73 %, corresponding to an increase of 372 % of mechanical power when compared with the ambient temperature conditions. For this machine, no thermal restrictions were verified, due to the high capacity of heat extraction of liquid nitrogen. Therefore, this maximum mechanical power point is only limited by the torque-speed sable zone.

Last but not the least, while the efficiency of the machine increases highly under wet cryogenic conditions for a higher torque, it seems unreasonable to use a standard motor for the same rated torque of the ambient temperature conditions. In the latter case, the increase of efficiency is lower and may not compensate the cryostat consumption that was not considered in the work.

V. CONCLUSION

In this work, an experimental assessment of the influence of cryogenic cooling in a fractional kilowatt induction motor, originally designed for ambient temperature operation, is performed. The experimental findings supported by the analytical procedure show that, in this fractional kilowatt induction motor, under ambient conditions, the stator Joule losses are the highest source of losses. Therefore, the high reduction of the stator resistance contributed to a high increase of efficiency, for the same stator current. Comparing the ambient temperature and cryogenic conditions, the maximum efficiency increased from 63 % to 85.2 % and the nominal torque increased from 0.72 Nm to 1.95 Nm. In addition, due to the excellent cooling capacities of the liquid nitrogen, that keeps the machine active parts below 77 K during operations, no thermal limitation was found for the whole stable zone of the torque-speed characteristic.

The machine could operate for one hour, immersed in liquid nitrogen, without experiencing any mechanical, electric, or thermal problems. Due to the presence of liquid nitrogen, the mechanical losses almost doubled at rated speed. The analytical methodology proposed to analyze the impact of the cryogenic cooling, based on the single-phase equivalent circuit parameters, was validated, and has shown to be a good tool to estimate the performance of the induction motor under cryogenic conditions.

The analysis proves that, while wet cryogenic conditions allow a higher efficiency and torque, it makes no sense to operate a conventional IM at cryogenic temperature to obtain the same rated power. In other words, to achieve the best efficiency at the desired torque, the machine design must be optimized for cryogenic conditions. Based on the accurate obtained results and considering that in literature there are few results of small/medium IMs, the authors decided to extend the proposed methodology of analysis to motors in the 1-15kW

range, both considering conventional and cryo-designed machines, in future research works.

The cryogenic cooling allows a higher increase of efficiency and loading capabilities, however it requires a complex cryostat for its implementation that may not justify the increase of the electrical machine efficiency and loading. This cannot be generalized and must be analyzed for each application. For instance, the cryogenic cooling can be advantageous in applications where a cryogenic fluid is already present, as in liquid natural gas pumping stations, or in future electric aircrafts where the liquid hydrogen can be used as fuel and as cryogenic coolant.

VI. References

[1] Commission Regulation (EU) 2019/1781, *Official Journal of the European Union*, L272/74 ed., October 2019.

[2] European Union: European Commission, "Report From The Commission To The European Parliament, The Council, The European Economic And Social Committe And The Committe Of The Regions Com (2021) 950 Final," *European Commission*, Brussels, 2021.

[3] NASA Aeronautics, "NASA Aeronautics Strategic Implementation Plan: 2019 Update"; Technical Report NP-2017-01-2352-HQ; National Aeronautics and Space Administration (NASA): Whasington, DC, USA, 2019.

[4] ASAB Projects. Single-aisle Turboelectric Aircraft with Aft Boundary-Layer Propulsion. https://sacd.larc.nasa.gov/asab/asab-projects-2/starc-abl/. Accessed: 2021-12-20.

[5] B. Sudha, V. Anusha and S. Sachin, "A review: high power density motors for electric vehicles," Journal of Physics: Conference Series, vol. 1706, pp. 012057, Dec. 2020.

[6] M. A. J. Kondelaji and M. Mirsalim, "Segmented-Rotor Modular Switched Reluctance Motor With High Torque and Low Torque Ripple," *IEEE Transactions on Transportation Electrification*, vol. 6, no. 1, pp. 62-72, March 2020.

[7] G. J. Li, X. Y. Ma, G. W. Jewell and Z. Q. Zhu, "Novel Modular Switched Reluctance Machines for Performance Improvement," in *IEEE Trans. Energy Conv*., vol. 33, no. 3, pp. 1255-1265, Sept. 2018

[8] B. Gamble, G. Snitchler, and T. MacDonald, "Full power test of a 36.5 MW HTS propulsion motor," IEEE trans. Applied Superconductivity, vol. 21, pp. 1083 – 1088, July 2011.

[9] X. Song et al., "Ground Testing of the World's First MW-Class Direct-Drive Superconducting Wind Turbine Generator," in *IEEE Trans. Energy Conv*., vol. 35, no. 2, pp. 757-764, June 2020.

[10] G. Messina, M. Yazdani-Asrami, F. Marignetti, and A. della Corte, "Characterization of HTS Coils for Superconducting Rotating Electric Machine Applications: Challenges, Material Selection, Winding Process, and Testing", in *IEEE Trans. Appl. Superconductivity*, vol. 31, no. 2, 5200310, Mar. 2021.

[11] F. Marignetti, S. Carbone, V. Delli Colli, and C. Attaianese, "Cryogenic Characterization of Copper-Wound Linear Tubular Actuators", in *IEEE Trans. Ind. Electron*., vol. 59, no. 5, pp. 2167-2177, May. 2012.

[12] F. Marignetti, V. Cavaliere, G. Giunchi, G. Messina, G. Celentano and A. Matrone, "Use of MgB_2 Superconductors for Excitation Field in Synchronous Machines—Part I: Bulk Magnets", *IEEE Trans. Appl. Superconductivity*, vol. 23, no. 4, 8002506, Aug. 2013.

[13] F. Marignetti, V. Cavaliere, G. Giunchi, G. Messina, C. Attaianese and A. Della Corte, "Use of MgB_2 Superconductors for Excitation Field in Synchronous Machines—Part II: Inserts", *IEEE Trans. Appl. Superconductivity*, vol. 23, no. 4, 8002606, Aug. 2013.

[14] X. Zhang, C. L. Bowman, T. C. O'Connell., K. S Haran, "Large electric machines for aircraft electric propulsion," *IET Electric Power Appl.*, vol. 12, nº 6, pp. 767-779, 1 July 2018.

[15] K. S Haran, S. Kalsi, T. Arndt, H. Karmaker, R. Badcock, B. Buckley, T. Haugan, M. Izumi, D. Loder, J. W. Bray, P. Masson and E. Wolfgang Stautner, "High power density superconducting rotating machines - development status and technology roadmap," *Superconductor Science and Technology*, vol. 30, nº 12, p. 123002, November 2017.

[16] L. Ai, G. Zhang, L. Jing, X. Xu and J. Si, "Behaviors of Axial and Radial Electromagnetic Force for Cryogenic Disk Motor," in *IEEE Trans. Energy Conv*., vol. 36, no. 2, pp. 874-882, June 2021.

[17] D. Miyagi, D. Otome, M. Nakano and N. Takahashi, "Measurement of Magnetic Properties of Nonoriented Electrical Steel Sheet at Liquid Nitrogen Temperature Using Single Sheet Tester," in *IEEE Transactions on Magnetics*, vol. 46, no. 2, pp. 314-317, Feb. 2010.

[18] X. Lv, D. Sun and L. Sun, "Determination of Iron Loss Coefficients of Ferromagnetic Materials Used in Cryogenic Motors," 2019 22nd International Conference on Electrical Machines and Systems (ICEMS), pp. 1-5, 2019.

[19] E. Ma, H. Wu, Y. Li, "Development and testing of a cryogenic induction motor with a novel Dewar structure", *Cryogenics*, Volume 116, 2021.

[20] A. Chengliu, H. Yuanfeng, W. Haifeng, G. Guobiao and D. Yumei, "Thermal analysis and optimization of the stator structure of a submerged cryogenic induction motor," 2014 IEEE Conference and Expo Transportation Electrification Asia-Pacific (ITEC Asia-Pacific), 2014.

[21] J. H. Redmond, and F. W. Bott. "Development of Cryogenic Electric Motors," *SAE Transactions*, vol. 72, 1964.

[22] C. Ai, Y. Huang and H. Wang, "Coupled Electromagnetic and Thermal Analysis of a 15kW Cryogenic Induction Motor for Submerged Liquefied Natural Gas Pumps," 2020 23rd International Conference on Electrical Machines and Systems (ICEMS), Hamamatsu, Japan, 2020.

[23] H. M. Kim, K. W. Lee, D. G. Kim, J. H. Park and G. S. Park, "Design of Cryogenic Induction Motor Submerged in Liquefied Natural Gas," in *IEEE Trans. Magnetics*, vol. 54, no. 3, pp. 1-4, March 2018.

[24] R. Shively, "Submerged cryogenic motor materials development," in IEEE Electrical Insulation Magazine, vol. 19, no. 3, pp. 7-11, May-June 2003.

[25] M. Biasion, J. F. P. Fernandes, P. J. C. Branco, S. Vaschetto, A. Cavagnino, A. Tenconi, "A Comparison of Cryogenic-Cooled and Superconducting Electrical Machines", IEEE Energy Conversion Congress & Expo, Oct. 10-14, 2021.

[26] R. A. Matula, "Electrical resistivity of copper, gold, palladium, and silver", *Journal of Physical and Chemical Reference Data*, vol. 8, pp. 1147-1298, 1979.

[27] A. Cavagnino, "Accuracy-Enhanced Algorithms for the Slot Leakage Inductance Computation of Double-Layer Windings," in IEEE Transactions on Industry Applications, vol. 53, no. 5, pp. 4422-4430, Sept.-Oct. 2017.

[28] A. Boglietti, A. Cavagnino and M. Lazzari, "Computational Algorithms for Induction-Motor Equivalent Circuit Parameter Determination—Part I: Resistances and Leakage Reactances," in *IEEE Trans. Ind. Electron*., vol. 58, no. 9, pp. 3723-3733, Sept. 2011.

[29] H. J. Hucek, K. E. Wilkes, K. R. Hanby, and J. K. Thompson. "Handbook on Materials for Superconducting Machinery". *Metals and Ceramics Information Center*, 1st edition, 1977.

[30] A. Boglietti, A. Cavagnino and M. Lazzari, "Computational Algorithms for Induction-Motor Equivalent Circuit Parameter Determination—Part II: Skin Effect and Magnetizing Characteristics," in *IEEE Trans. Ind. Electron*., vol. 58, no. 9, pp. 3734-3740, Sept. 2011.

[31] X. Lv, D. Sun and L. Sun, "Determination of Iron Loss Coefficients of Ferromagnetic Materials Used in Cryogenic Motors," 2019 22nd International Conference on Electrical Machines and Systems (ICEMS), pp. 1-5, 2019.